Acoustic plasmons and doping evolution of Mott physics in resonant inelastic x-ray scattering from cuprate superconductors

R. S. Markiewicz,[1] M. Z. Hasan,[2] and A. Bansil[1]
[1]*Physics Department, Northeastern University, Boston, Massachusetts 02115, USA*
[2]*Joseph Henry Laboratories of Physics, Department of Physics, Princeton University, Princeton, New Jersey 08544, USA and Princeton Center for Complex Materials, Princeton University, Princeton, New Jersey 08544, USA*
(Received 20 December 2007; published 25 March 2008)

By incorporating a long-range Coulomb interaction into the framework of the one-band Hubbard model, we delineate how the low-energy plasmon around 1 eV, which is a universal feature of the charge dynamics of the cuprates, manifests itself in the resonant inelastic x-ray scattering (RIXS) spectra. The long-range Coulomb interaction in the doped system controls the form of the intraband RIXS dispersion near the Brillouin zone center around the Γ point. The out-of-plane momentum transfer component q_z is found to play a key role in determining whether or not the RIXS spectrum shows a plasmon-related gap at Γ.

DOI: 10.1103/PhysRevB.77.094518 PACS number(s): 78.70.Ck, 75.50.Ee, 74.72.−h, 71.45.Gm

I. INTRODUCTION

Resonant inelastic x-ray scattering (RIXS) is rapidly emerging as a unique tool for investigating charge excitations in wide classes of materials. In the strongly correlated cuprates, RIXS has been used to probe the doping evolution of Mott physics, which lies at the heart of developing an understanding of how the insulating state turns into a high-temperature superconductor. In this connection, it is important to understand how the RIXS spectrum is influenced by the presence of the anomalously low-energy plasmon at around 1 eV, which is a universal feature of the charge dynamics of the cuprates. Plasmon physics has been accessed traditionally via optical and electron energy loss spectroscopies (EELSs).[1–3] However, optical studies are limited to zero momentum transfer, while RIXS can probe excitations over a wide range of momenta and energies. On the other hand, EELS involves a charged particle going in and out of the sample and suffers from multiple scattering effects, but these complications are ameliorated in a RIXS experiment, which involves the scattering of a photon.

In this paper, we delineate how the low-energy plasmon manifests itself in the RIXS spectrum of the cuprates. We proceed by incorporating a long-range Coulomb interaction into the framework of the one-band Hubbard model. Our analysis focuses for simplicity on properties of the loss function, whose energy and momentum dependence is shown to be related intimately to that of the RIXS spectrum. Illustrative results are presented for insulating $Sr_2CuO_2Cl_2$ (SCOC) as well as for (overdoped) metallic $Bi_2Sr_2CuO_6$ (Bi2201). The long-range Coulomb interaction yields little effect in the insulating case, where the spectrum is dominated by interband transitions across the Mott gap. In contrast, the plasmon can strongly modify the intraband spectrum in the doped system near Γ, depending on the value of the out-of-plane momentum transfer component q_z. For $q_z=0$, we find surprisingly that the plasmon dominates so that the RIXS spectrum displays a gap at the Γ point even though the underlying electronic spectrum does not possess a gap. For $q_z\neq 0$, the acoustic plasmon leads to a softening of the RIXS spectrum around the Γ point. These results bear directly on the interpretation of the RIXS spectra and their implications for the doping evolution of Mott physics in the cuprates. To our knowledge, the role of the plasmon in creating a gap in the RIXS spectrum around Γ and the key importance of the out-of-plane momentum transfer component q_z in this connection have not been recognized previously in the literature.

II. FORMALISM

A. Resonant inelastic x-ray scattering cross section

In a RIXS process, a photon scatters resonantly to another state, leaving behind an electron-hole (e-h) excitation of well defined momentum $\mathbf{q}$ and energy ω. The K-edge RIXS intensity, which is the focus of this paper, is given by the general expression[4,5]

$$I_{RIXS}(\mathbf{q},\omega,\omega_i) = (2\pi)^3 N |w(\omega,\omega_i)|^2 \sum_{jj',\mathbf{k}} \chi''_{0jj'}(\mathbf{q},\mathbf{k},\omega) \times |P_{j,j'}(\mathbf{q},\mathbf{k},\omega)|^2, \quad (1)$$

where

$$\chi''_{0jj'}(\mathbf{q},\mathbf{k},\omega) = \delta[\omega + E_j(\mathbf{k}) - E_{j'}(\mathbf{k}+\mathbf{q})] n_j(\mathbf{k})[1 - n_{j'}(\mathbf{k}+\mathbf{q})] \quad (2)$$

is related to the joint density of states (JDOS) factor $\chi''_{0jj'}(\mathbf{q},\omega)=\Sigma_{\mathbf{k}}\chi''_{0jj'}(\mathbf{q},\mathbf{k},\omega)$ as discussed in Refs. 4 and 5, and

$$w(\omega,\omega_i) = \sum_{\mathbf{k}_1} \frac{|\gamma|^2}{D(\omega_i,\mathbf{k}_1) D(\omega_f,\mathbf{k}_1)}. \quad (3)$$

Here, $D(\omega,\mathbf{k})=\omega+\epsilon_{1s}-\epsilon_{4p}(\mathbf{k})+i\Gamma_{1s}$, the Cu $1s$ band is assumed dispersionless at energy ϵ_{1s} with lifetime broadening Γ_{1s}, and the Cu $4p$ band $\epsilon_{4p}(\mathbf{k}_1)$ is modeled by a two-dimensional (2D) tight binding band with nearest neighbor hopping. Polarization effects arise via the Cu $1s$-$4p$ transition factor γ, which is taken for simplicity to be a constant. The quantities $P_{j,j'}$ in Eq. (1) are given by the expression

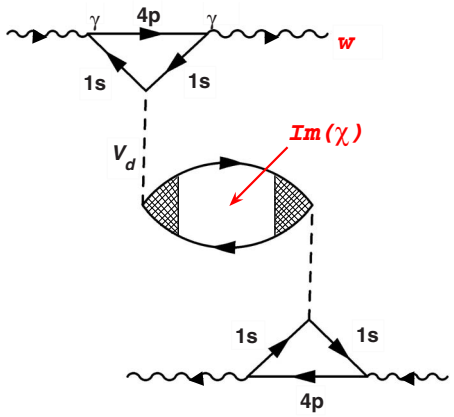

FIG. 1. (Color online) Lowest-order Keldysh diagram for K-edge RIXS process, after Ref. 5.

$$P_{j,j'}(\mathbf{q},\mathbf{k},\omega) = \sum_{\ell,\sigma,\sigma'} e^{i\mathbf{q}\cdot\mathbf{R}_\ell} V_\ell X^j_{\ell\sigma}(\mathbf{k}) \Lambda_{\sigma,\sigma'}(\omega,\mathbf{q}) X^{j'}_{\ell\sigma'}(\mathbf{k}+\mathbf{q}). \tag{4}$$

Here, σ is the electron spin index, $\mathbf{R}_\ell$ is the distance from the core hole to atom ℓ, and $X^j_{\ell,\sigma}$ are the eigenvectors of the energy bands j with respect to the different atomic states.

RIXS intensity of Eq. (1) is based on the leading order Keldysh diagram of Fig. 1, where the upper or the lower triangle in the figure represents the RIXS amplitude.[5] In particular, The electron-photon vertex γ and the $1s$ and $4p$ propagators given by $D(\omega,\mathbf{k})$ combine to produce the weight w of Eq. (3). The low-energy electron-hole pair depicted by the polarization diagram in the middle of the figure is assumed to couple predominantly to the core hole, and the $4p$ state is assumed to be a delocalized spectator. We emphasize that the core hole can, in general, induce a complex rearrangement of electronic states, including carrier hopping processes. Here, we treat the core hole in lowest order as a bare Coulomb energy V_ℓ between an electron on site ℓ and the core hole, with V_d denoting the corresponding onsite energy. This Coulomb potential leads to a mixing of various onsite orbitals, but it does not allow hopping between different sites. Notably, the present formulation does not include effects of the electron-hole interaction in the final state.

B. Relation to electron energy loss spectroscopy

Here, we demonstrate a close connection between the EELS and RIXS response functions within the framework of the one-band Hubbard model. Recall that EELS measures

$$I_{EELS}(q,\omega) \propto q^2 L(\mathbf{q},\omega), \tag{5}$$

where the loss function is

$$L(\mathbf{q},\omega) = \mathrm{Im}[-1/\epsilon(\mathbf{q},\omega)] \tag{6}$$

and the dielectric function is

$$\epsilon(\mathbf{q},\omega) = \epsilon_0 + V(\mathbf{q})\chi_0(\mathbf{q},\omega), \tag{7}$$

in terms of the bare charge susceptibility $\chi_0(\mathbf{q},\omega)$ and the Fourier transform $V(\mathbf{q})$ of the Coulomb interaction, which includes the effect of the onsite Hubbard term U. For our model of a layered compound, $V(\mathbf{q})$ is discussed in more detail in the Appendix. The plasmon dispersion $\omega_p(\mathbf{q})$ is defined via peaks of the loss function L at various momenta $\mathbf{q}$.

Consider the factor P of Eq. (4). In the antiferromagnetic (AFM) state, the eigenvectors $X^j_{\ell,\sigma}$ reduce to the (AFM) Bogoliubov coherence factors v and u of the lower (LMB) and upper magnetic bands (UMB), and $P_{j,j'}$ becomes a 2×2 matrix, where $j=1$ denotes the LMB and $j=2$ the UMB. In the paramagnetic state, the index j is not needed so that $P_{j,j'}$ is a $\mathbf{k}$ independent scalar (denoted by P), $X^j_{\ell,\sigma}=1$, and if the vertex correction Λ is neglected [i.e., $\Lambda_{\sigma,\sigma'}(\omega,\mathbf{q})=\delta_{\sigma,\sigma'}$], Eq. (4) yields $P=\bar{V}(\mathbf{q})$, the Fourier transform of the total Coulomb interaction of the core hole. The corresponding result when the vertex correction is approximated by a random phase approximation bubble sum[6,7] is $P=\epsilon(\mathbf{q},\omega)^{-1}\bar{V}(\mathbf{q})$, where the dielectric function is given by Eq. (7). Note that $\bar{V}(\mathbf{q})$ differs from $V(\mathbf{q})$ defined earlier in that $\bar{V}(\mathbf{q})$ is the interaction energy of an electron with the core hole, while $V(\mathbf{q})$ is that between two electrons. Assuming that $\bar{V}(\mathbf{q})$ and $V(\mathbf{q})$ differ only in the onsite interaction, it follows that $\bar{V}(\mathbf{q})=V(\mathbf{q})+V_d-U$. Introducing $\hat{V}(\mathbf{q})\equiv\bar{V}(\mathbf{q})^2/V(\mathbf{q})$, the one-band (paramagnetic) RIXS response becomes

$$I_{RIXS}(\mathbf{q},\omega,\omega_i) = (2\pi)^3 N |w(\omega,\omega_i)|^2 \hat{V}(\mathbf{q}) L(\mathbf{q},\omega), \tag{8}$$

with the same loss function

$$L(\mathbf{q},\omega) = \mathrm{Im}[-1/\epsilon(\mathbf{q},\omega)] = \frac{V(\mathbf{q})\chi_0''(\mathbf{q},\omega)}{|\epsilon(\mathbf{q},\omega)|^2}. \tag{9}$$

III. PLASMON EFFECTS

Equation (8) shows clearly that the low-energy plasmon involved in the loss function not only controls the behavior of the EELS spectrum via Eq. (5), but also plays a significant role in modifying the RIXS spectrum.[8] Accordingly, we turn now to consider the nature of the loss function in the cuprates with the examples of SCOC and Bi2201 in order to highlight the effects of the plasmon. For this purpose, the model one-band dispersion (Cu only) employed is of the form[9]

$$\epsilon_{\mathbf{k}} = -2t[c_x(a)+c_y(a)] - 4t' c_x(a)c_y(a) - 2t''[c_x(2a)+c_y(2a)] - 4t'''[c_x(2a)c_y(a)+c_y(2a)c_x(a)], \tag{10}$$

where $c_\alpha(na)=\cos(nk_\alpha a)$, for $\alpha=x$ or y, n is an integer, and a is the in-plane lattice constant. The values of the hopping parameters t, t', t'', and t''' for SCOC and Bi2201 used in this study are the same as those given previously in Ref. 9.

A. Coulomb interaction

The key is the treatment of the Coulomb interaction (see Appendix for details), which we decompose as[10]

$$V(\mathbf{q}) = V_{2D} + V_z, \tag{11}$$

with

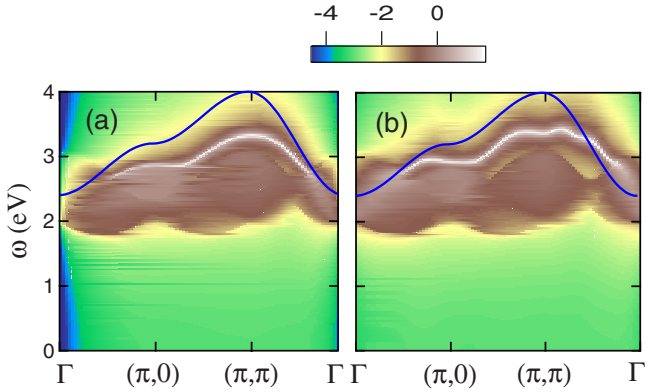

FIG. 2. (Color online) Calculated loss function for insulating SCOC as a function of energy transfer ω along the Γ-$(\pi,0)$-(π,π)-Γ high symmetry line in the Brillouin zone. Results for two different model treatments of the Coulomb interaction are shown: (a) only the short-range onsite Hubbard U term and (b) the full $V(q)$ of Eq. (9). Experimental plasmon dispersion obtained from EELS data (Ref. 3) is given by solid blue lines for reference in both panels (a) and (b). Note that intensities are plotted on a logarithmic scale.

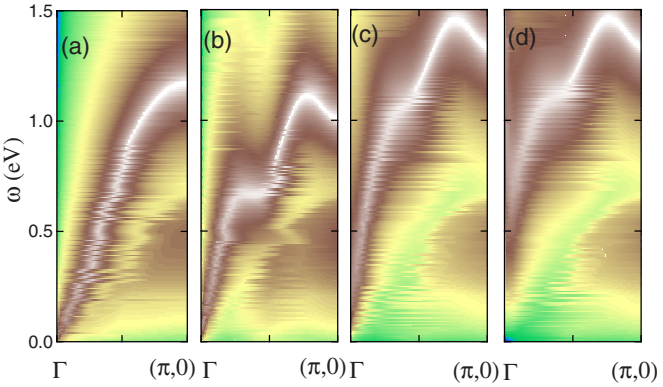

FIG. 3. (Color online) Calculated loss function for overdoped Bi2201 using four different ranges of the Coulomb potential, all restricted to $q_z=0$. Results in (a)–(d) are for an increasing range of the potential as follows: (a) only the onsite term U, (b) in-plane short-range term V_{2D}^{sr}, (c) total in-plane term V_{2D}, and (d) the full $V(q)$. The color scheme is the same as in Fig. 2.

$$V_{2D} = V_{2D}^{sr} + V_{2D}^{lr}. \tag{12}$$

Here, V_{2D} is the contribution within a single plane and V_z is the correction from all other planes. V_{2D} is further broken up into a short-range part $V_{2D}^{sr}(\mathbf{q})$, which is defined by taking a discrete sum over sites within a sphere of radius R_0 and includes the onsite U term. The long-range part, $V_{2D}^{lr}(\mathbf{q})$, is evaluated by taking a continuous Fourier integral extending from R_0 to ∞. We emphasize that while the intralayer part V_{2D} depends only on the in-plane momentum components q_x and q_y, the interlayer part V_z also possesses an important dependence on q_z,[11]

$$V_z(\mathbf{q}) = \frac{2\pi e^2}{a^2 q_\parallel \epsilon_0}\left[\frac{\cos(q_z c) - e^{-q_\parallel c}}{\cosh(q_\parallel c) - \cos(q_z c)}\right], \tag{13}$$

with $q_\parallel = \sqrt{q_x^2 + q_y^2}$. The q_z dependence in Eq. (13) is responsible for generating an acoustic branch in the plasmon spectrum of a quasi-2D material. In the computations reported in this study, for simplicity, we have taken all contributions in Eqs. (11) and (12) to be of the screened Coulomb form $V(r) = e^2/\epsilon_0 r$ (except for the onsite U). The model parameters appropriate to the cuprates are $U=2$ eV and the background dielectric constant $\epsilon_0 = 6$.[12] R_0 is taken as four lattice constants, but the results are not sensitive to these details.

B. Plasmons and long-range interaction

Figure 2 presents the computed loss spectrum for SCOC. The system is assumed to be in the AFM insulating state so that the electronic spectrum consists of the lower and upper magnetic bands, which are separated by a gap of $\sim U$. The loss function resulting from the inclusion of only the onsite Hubbard U term in the calculations is shown in (a). The corresponding result for the full $V(q)$, including its longer-range part, is shown in (b). Although the theoretical spectra in (a) and (b) are qualitatively similar, a q-dependent shift to higher energies can be seen in (b) due to the effect of the long-range Coulomb interaction.[13] This is especially evident near the zone center along the $\Gamma-(\pi,\pi)$ symmetry line where the peak of the spectrum (whitish trace) drops below the blue reference line (experimental plasmon dispersion) in (a), but it mostly lies above the blue line in (b).

C. Acoustic plasmons

Figure 3 discusses with the example of Bi2201 the case of an overdoped cuprate where the magnetic gap has collapsed. All results in Fig. 3 are based on setting $q_z=0$ in the potential function; we return below to address the significant effects of the $q_z \neq 0$ components. The four panels in the figure refer to the use of different ranges of the screening potential in the loss function computation. In particular, the potential range is increased in going from (a) to (d) via the use of different potential functions as follows: (a) only the onsite term U, (b) the effect of the in-plane short-range term V_{2D}^{sr}, which includes U, (c) effect of the total in-plane term V_{2D}, and (d) the full $V(q)$. We see that as the range of the potential increases from being just the onsite Hubbard U term in (a) to the full $V(q)$ in (d), the plasmon spectrum generally shifts in a systematic manner to higher energies.[14] The difference between panels (a) and (d) is very striking near the zone center at Γ in that the dispersion extrapolates to zero energy at Γ in (a) for the short-range potential, but in sharp contrast, the long-range case in (d) displays the presence of a gap ω_p at Γ. This difference is readily understood. For the pure Hubbard model, the loss function is simply the q-resolved JDOS for the electronic band. However, in a single band there can be no vertical (interband) transitions, which forces the JDOS to start from zero energy at Γ. Long-range screening then opens a gap at Γ associated with the plasmon energy ω_p.

Insight into the role of the plasmon in the results of Fig. 3 can be obtained by recalling some generic properties of the lower-dimensional plasmons.[11,15] In the present context, it is helpful to consider a simple 2D model with isotropic dispersion and circular Fermi surface, where the high frequency

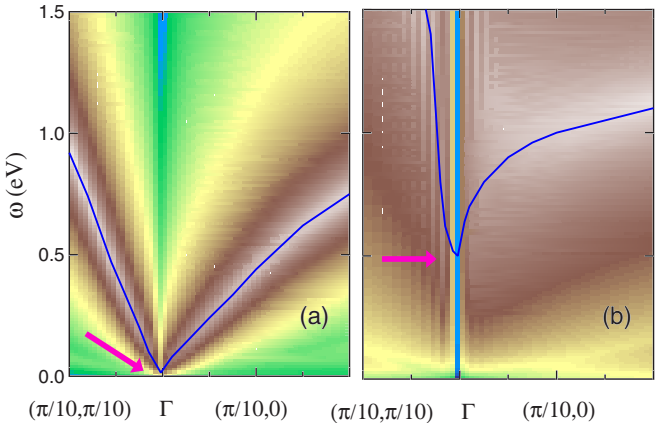

FIG. 4. (Color online) Calculated loss spectra for Bi2201 illustrating effect of q_z: (a) $q_z=2\pi/c$; (b) $q_z=0$. Blue solid lines show positions of the spectral peaks. The arrows show a peak position at Γ. The logarithmic color scale is the same as in Fig. 2.

susceptibility is straightforwardly shown to take the form $\chi(\mathbf{q},\omega)\sim -n_0 q_\parallel^2/m\omega^2$, where n_0 is the three-dimensional (3D) density, so that

$$\omega_p^2 = n_0 V_{\mathbf{q}} q_\parallel^2/\epsilon_0 m. \tag{14}$$

Equation (14) leads to several special cases of interest depending on V_q. For the *pure Hubbard model*, $V_{\mathbf{q}}=Ua^2c$ is a constant (c is the interlayer spacing of CuO_2 planes) and Eq. (14) has the form of an *acoustic* plasmon, $\omega_p\sim q_\parallel$, as is the case in panels (a) and (b) of Fig. 3. For a *single layer cuprate with long-range Coulomb interaction* $V_{2D}(q)$ of Eq. (12), the U term can be neglected as $q\to 0$, so that

$$\omega_p^2 = \frac{2\pi n_{2D} e^2 q_\parallel}{\epsilon_0 m}, \tag{15}$$

yielding the anomalous dispersion $\omega_p\sim q_\parallel^{1/2}$ of Fig. 3(c). For a *layered cuprate with the long-range Coulomb interaction* $V(q)$ of Eq. (11),

$$\omega_p^2 = \frac{4\pi n_0 e^2 q_\parallel^2}{\epsilon_0 m q^2}. \tag{16}$$

When $q_z=0$, $q\to q_\parallel$ and the familiar 3D form of ω_p is recovered in Eq. (16), leading to the results of Fig. 3(d). However, when $q_z\neq 0$, $\omega_p\to 0$ as $q_\parallel\to 0$, leading to an acoustic plasmon, as discussed below in connection with Fig. 4.

Figure 4 shows that the behavior of the loss spectrum in the vicinity of the Γ point is sensitive to the value of the out-of-plane momentum component q_z. For $q_z\neq 0$, the spectral peak in Fig. 4(a) given by the solid line essentially goes to zero energy at Γ, rather like the case of Fig. 3(a), which includes just the onsite Hubbard interaction. In other words, for $q_z\neq 0$ the acoustic plasmon associated with long-range Coulomb interaction, dominates the loss spectrum around Γ consistent with our discussion of Eq. (16) above. In sharp contrast, for $q_z=0$ in Fig. 4(b), the acoustic plasmon is absent, and the peak of the spectrum no longer goes to zero energy at Γ, but lies at a finite energy of around 0.5 eV, as marked by the red arrow.

D. Experimental consequences

As for confronting our theoretical predictions with experiments, we are not aware of any systematic RIXS study in the cuprates as a function of q_z, although recent RIXS results of Refs. 16–18 on the electron-doped $Nd_{2-x}Ce_xCuO_4$ (NCCO) are relevant because the data set of Ref. 16 was taken at $q_z\approx 0$ and that of Refs. 17 and 18 at $q_z=12.5(4\pi/c)$, which corresponds to $q_z\neq 0$ when reduced into the first Brillouin zone.[19] In the $q_z=0$ case, the spectra display [see Fig. 5(c) of Ref. 16] the presence of a prominent band of interband RIXS transitions, which softens significantly with doping, but does not show a full collapse around Γ at optimal doping, much like the theoretically predicted behavior of Fig. 4(b).[20] On the other hand, the $q_z\neq 0$ data [see Fig. 2(d) of Ref. 17 and Fig. 2 of Ref. 18] in the optimally doped NCCO display a RIXS band, which would appear to extrapolate to near zero energy around Γ, similar to our computed spectra of Fig. 4(a). Notably, optical spectra on $Pr_{2-x}Ce_xCuO_4$, a closely related electron-doped cuprate,[21] show that by 15% doping (see Fig. 4 of Ref. 21), a large portion of the spectral weight shifts into a broad peak below 1 eV, in sharp contrast to the $q_z=0$ RIXS data. This, however, is to be expected since optical absorption is insensitive to (longitudinal) plasmon physics while RIXS is not.

IV. CONCLUSIONS

In conclusion, by incorporating a long-range Coulomb interaction into the Hubbard model, we have delineated the important role of acoustic plasmons in modifying the RIXS spectra of the doped cuprates. Most dramatic modifications in the spectrum occur in the low momentum region around the Γ point and show sensitivity to the out-of-plane momentum transfer component q_z. Our study bears on the interpretation of the RIXS spectra from the cuprates and shows how RIXS can probe the properties of acoustic plasmons in these and related materials. Such studies should also enable a quantitative assessment of the possible relevance of acoustic plasmons in the mechanism of high-temperature superconductivity[22] and of the importance of long-range Coulomb interaction on the Mott transition.[23]

ACKNOWLEDGMENTS

This work is supported by the U.S. Department of Energy Contracts No. DE-FG02-07ER46352 and No. DE-AC03-76SF00098, and benefited from the allocation of supercomputer time at NERSC and Northeastern University's Advanced Scientific Computation Center (ASCC). The work at Princeton is supported by the DOE Grant No. DE-FG-02-05ER46200.

APPENDIX: LONG-RANGE COULOMB INTERACTION

The treatment of the long-range Coulomb interaction $V(r)$ for the correlated electronic system in a layered structure requires some care.[10] We model $V(\mathbf{r})=\Sigma_i \tilde{\mathbf{V}}(\mathbf{R}_i)\delta(\mathbf{r}-\mathbf{R}_i)$, so $V(\mathbf{q})=\Sigma_i \tilde{\mathbf{V}}(\mathbf{R}_i)\exp[i(\mathbf{q}\cdot\mathbf{R}_i)]$. $V(\mathbf{R}_i)$ is taken as an onsite Hubbard term $\tilde{V}(0)=U=2$ eV plus screened Coulomb contribu-

tion for $R_i \neq 0$ given by $\tilde{V}(\mathbf{R}_i)=\mathbf{e}^2/[\epsilon_0 \mathbf{R}_i]$, using a background dielectric constant $\epsilon_0=6$. We define $\mathbf{R}_i=\mathbf{R}_{i0}+\ell c\hat{\mathbf{z}}$, where $\mathbf{R}_{i0}$ is a two-dimensional lattice vector, $\hat{\mathbf{z}}$ is a unit vector perpendicular to the layers, ℓ is a positive or negative integer or zero, and a and c are the in-plane and perpendicular lattice constants. $V(\mathbf{r})$ can now be expressed as a sum over layer contributions: $V(\mathbf{r})=\Sigma_\ell \mathbf{V}_\ell(\mathbf{r})$, with

$$V_\ell(\mathbf{r}) = \sum_i \tilde{\mathbf{V}}_\ell(\mathbf{R}_{i0})\delta(\mathbf{r}-[\mathbf{R}_{i0}+\ell \mathbf{c}\hat{\mathbf{z}}]), \tag{A1}$$

with $\tilde{V}_\ell(\mathbf{R}_{i0})=\tilde{\mathbf{V}}(\mathbf{R}_{i0}+\ell \mathbf{c}\hat{\mathbf{z}})$. $V_{q,\ell}$ can then be obtained via a lattice Fourier transform.

To simplify the resulting expression, while still capturing properly the long-range $(q\rightarrow 0)$ part of $V_{q,\ell}$, we employ a Lorentz cavity approximation by summing the contributions of all ℓ-plane Cu terms for $r \leqslant R_\ell$ and approximating the remaining contributions for $r>R$ by a continuum in order to recover the correct $q\rightarrow 0$ limit of $V_{q,\ell}$. Thus,

$$V_{q,\ell} = \sum_i{}' V_\ell(\mathbf{R}_{i0})\mathbf{e}^{-i\mathbf{q}\cdot\mathbf{R}_i} + \mathbf{V}^{lr}_{\mathbf{q},\ell}, \tag{A2}$$

where the prime means $\mathbf{R}_{i0} \leqslant \mathbf{R}_\ell$ and

$$V^{lr}_{q,\ell} = e^{-iq_z\ell c}\int_{R_\ell}^{\infty} \frac{d^2r}{a^2}\frac{e^2}{\epsilon_0\sqrt{r^2+(\ell c)^2}}e^{-i\mathbf{q}_\parallel\cdot\mathbf{r}} = \frac{2\pi e^2 e^{-iq_z\ell c}}{\epsilon_0 a^2 q_\parallel}J(q_\parallel,\ell), \tag{A3}$$

with

$$J(q_\parallel,\ell) = \int_{q_\parallel R_\ell}^{\infty} \frac{xJ_0(x)dx}{\sqrt{x^2+(q_\parallel \ell c)^2}}. \tag{A4}$$

For $\ell=0$, the integral can be done exactly,

$$J(q_\parallel,0) = \left[1 - xJ_0(x) + \frac{\pi x}{2}\{J_0(x)H_1(x) - J_1(x)H_0(x)\}\right]_{x=q_\parallel R_0}, \tag{A5}$$

where H_i are Struve functions.[24] In the actual calculations, we take $R_0=4a$ and $R_\ell=0$ for $\ell \neq 0$, in which case

$$J(q_\parallel,\ell) = e^{-q_\parallel \ell c}. \tag{A6}$$

Finally, by summing over $V_{q,\ell}$ for $\ell \neq 0$, one obtains the net interplane contribution $V_z(\mathbf{q})$ of Eq. (13).

[1] I. Bozovic, Phys. Rev. B **42**, 1969 (1990).

[2] N. Nücker, H. Romberg, S. Nakai, B. Scheerer, J. Fink, Y. F. Yan, and Z. X. Zhao, Phys. Rev. B **39**, 12379 (1989); M. R. Norman, M. Randeria, H. Ding, and J. C. Campuzano, *ibid.* **59**, 11191 (1999); L. Hedin and J. D. Lee, *ibid.* **64**, 115109 (2001).

[3] Y. Y. Wang, F. C. Zhang, V. P. Dravid, K. K. Ng, M. V. Klein, S. E. Schnatterly, and L. L. Miller, Phys. Rev. Lett. **77**, 1809 (1996).

[4] R. S. Markiewicz and A. Bansil, Phys. Rev. Lett. **96**, 107005 (2006).

[5] T. Nomura and J.-i. Igarashi, Phys. Rev. B **71**, 035110 (2005).

[6] J.-i. Igarashi, T. Nomura, and M. Takahashi, Phys. Rev. B **74**, 245122 (2006).

[7] In particular, the results of Ref. 6 reduce to the present form by using (in the notation of Ref. 6) $\epsilon(\mathbf{q},\omega)=1+2U_d F^{\sigma}_{11}(q)$.

[8] Note that Eq. (8) has only been established for the paramagnetic state of a one-band Hubbard model.

[9] R. S. Markiewicz, S. Sahrakorpi, M. Lindroos, Hsin Lin, and A. Bansil, Phys. Rev. B **72**, 054519 (2005).

[10] R. S. Markiewicz and A. Bansil, Phys. Rev. B **75**, 020508(R) (2007).

[11] A. C. Sharma and I. Kulshrestha, Phys. Rev. B **46**, 6472 (1992).

[12] These parameters are taken to be doping independent, with screening incorporated via the dielectric constant.

[13] Interestingly, the upward shift of the spectrum in Fig. 2(b) would appear as an increase in the effective value of U in a pure Hubbard model.

[14] Oscillations in the plasmon dispersion in Figs. 3(b)–3(d) are due to the sharp cutoff R_0 used in computing the potential. These oscillations become smaller as the value of R_0 is increased.

[15] G. Giuliani and G. Vignale, *Quantum Theory of the Electron Liquid* (Cambridge University Press, Cambridge, 2005), p. 202.

[16] Y. Li, D. Qian, F. Gong, L. Wray, Y. Kaga, T. Sasagawa, H. Takagi, H. Eisaki, S. Uchida, R. S. Markiewicz, A. Bansil, and M. Z. Hasan, arXiv:0704.3111 (unpublished).

[17] K. Ishii, K. Tsutsui, Y. Endoh, T. Tohyama, S. Maekawa, M. Hoesch, K. Kuzushita, M. Tsubota, T. Inami, J. Mizuki, Y. Murakami, and K. Yamada, Phys. Rev. Lett. **94**, 207003 (2005).

[18] K. Ishii, K. Tsutsui, Y. Endoh, T. Tohyama, S. Maekawa, M. Hoesch, K. Kuzushita, T. Inami, M. Tsubota, K. Yamada, Y. Murakami, and J. Mizuki, in *Low Temperature Physics: 24th International Conference on Low Temperature Physics*, edited by Y. Takano, S. P. Hershfield, S. O. Hill, P. J. Hirschfeld, and A. M. Goldman (AIP, Melville, NY, 2006), p. 403.

[19] While the dielectric constant possesses the periodicity of the Brillouin zone (BZ), the matrix element does not. Therefore, the RIXS spectra will, in general, be different in various BZs. This BZ dependence of the spectrum is not considered in the present calculations.

[20] Notably, the leading edge in Fig. (5c) of Ref. 16, as well as in our Fig. 4(b), appears to show a collapse at Γ. (The calculated leading edge collapse can be enhanced by averaging the RIXS spectra over a finite q_z range.)

[21] T. Arima, Y. Tokura, and S. Uchida, Phys. Rev. B **48**, 6597 (1993).

[22] J. Ruvalds, Phys. Rev. B **35**, 8869 (1987); V. Z. Kresin and H. Morawitz, *ibid.* **37**, 7854 (1988).

[23] M. Capello, F. Becca, S. Yunoki, and S. Sorella, Phys. Rev. B **73**, 245116 (2006).

[24] I. S. Gradshteyn and I. M. Ryzhik, *Table of Integrals, Series, and Products* (Academic, Orlando, 1980).